# MODELING RESULTS FOR THE ALBA BOOSTER

G. Benedetti, D. Einfeld, U. Iriso, J. Marcos, Z. Martí, M. Muñoz, M. Pont
CELLS-ALBA, E-08290 Cerdanyola del Vallès, Spain

*Abstract*

The 3rd generation light source ALBA is in the process of being commissioned. The full energy 3 GeV booster synchrotron was commissioned during 2010, ramping the beam extracted from the linac at an energy of 110 MeV to the 3 GeV required for injection into the storage ring. The lattice is based in combined function bending magnets, providing a small emittance beam at extraction. This paper reviews the agreement between the optics modeling and the measures performed during the commissioning, with special regard to the tune, chromaticity and emittance measurement along the ramping process. The results from the magnetic measurements of the combined magnets during the ramping are included in the model to explain the movement of the tunes during the ramp.

## INTRODUCTION

The ALBA booster synchrotron is a modified FODO lattice structure based on unit cells consisting of defocusing combined dipoles and focusing quadrupoles and matching cells with a shorter combined dipole and three families of quadrupoles [3]

The calibrations of the integrated field in the dipoles and of the gradient strength of the quadrupoles determine respectively the ring energy and optics (tunes, emittance...). A precise modeling of the excitation curves of the magnets both at low and high current regime is crucial in a booster with such a variety of magnets to set the correct waveforms to obtain the working point and beam size along the ramp as close as possible to the needed values.

Table 1: Design parameters of the ALBA Booster.

| | | |
|---|---|---|
| Injection energy | 100 | MeV |
| Extraction energy | 3.0 | GeV |
| Circumference | 249.6 | m |
| Emittance at injection | 150 | nm·rad |
| Emittance at 3 GeV | 9 | nm·rad |
| Energy spread at injection | 0.005 | ... |
| Energy spread at extraction | 0.001 | ... |
| Betatron tunes $Q_x/Q_y$ | 12.42 / 7.38 | ... |
| Maximum betas $\beta_x/\beta_y$ | 11.2 / 11.7 | m |
| Maximum dispersion $D_x$ | 0.47 | m |
| Natural chromaticities $\xi_x/\xi_y$ | -17 / -10 | ... |
| Momentum compaction $\alpha_c$ | 0.0036 | ... |
| RF frequency | 500 | MHz |
| Harmonic number | 416 | ... |
| Repetition rate | 3.125 | Hz |

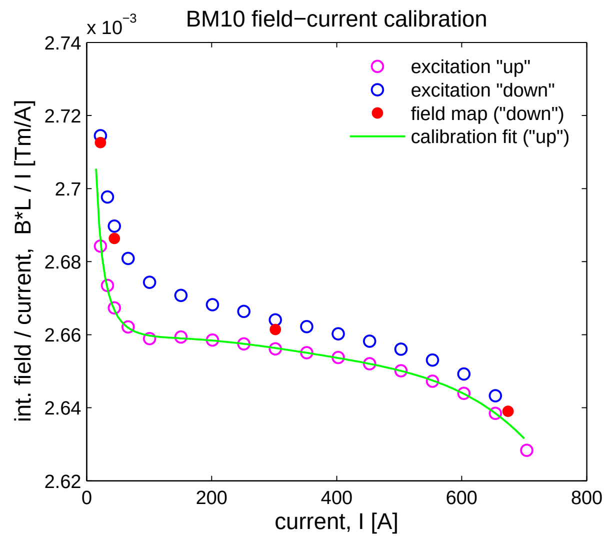


Figure 1: Long dipole BM10. Integrated field over current as a function of the excitation current.

## MODEL CALIBRATION

The calibration constants of the fields with respect to the powered currents used in the model are based in the magnetic measurements.

### *Combined gradient dipoles*

During the magnetic measurements, two excitation curves of the field $B_y$ at a point in the homogeneous region against the powered current $I$ were measured increasing the current up to 700 A (curve "up" corresponding to the accelerating cycle) and then decreasing it back to zero (curve "down").

Moreover, field map measurements in the mid plane were performed at four current set points between 670 A and 22 A taken in a descending excitation curve. The field maps data were used to determine the quadrupolar and sextupolar components along the nominal trajectory.

Figure 1 depicts the ratio of the field over the current for the two measured excitation curves "up" and "down" and the four measured field maps in the long bendings.

The field-to-current calibration of the model have been determined by fitting the ascending curve with a $5^{th}$ order polynomial (Eq. 1) to precisely reproduce the curve at both low and high current. The non-linear behaviour is very important al low energy for the injection working point and at high current to match the energy of the storage ring.

The gradient-to-current calibration constants have been determined by assuming that the bending gradient scales proportionally to the measured excitation "up" curve of the field (Eq. 2).

$$\int B \cdot ds\ [\mathrm{T \cdot m}] = b_0 + b_1\, I[A] + b_2\, I^2 + b_3\, I^3 + b_4\, I^4 + b_5\, I^5 \quad (1)$$

$$\int G \cdot ds\ [\mathrm{T}] = 2.6294 \cdot \int B \cdot ds\ [\mathrm{T \cdot m}] \quad (2)$$

$$k = \frac{1}{\rho} \frac{\int G \cdot ds}{\int B \cdot ds} = -0.22946\ [\mathrm{m^{-2}}] \quad (3)$$

### *Quadrupoles*

Figure 2 shows the gradient over current factor for one of the quadupoles measured from 1 A to the maximum of 180 A. As for the dipoles, the calibration constants have been fitted with a $5^{th}$ order polynomial to reproduce the nonlinear behaviour due to the remanent field.

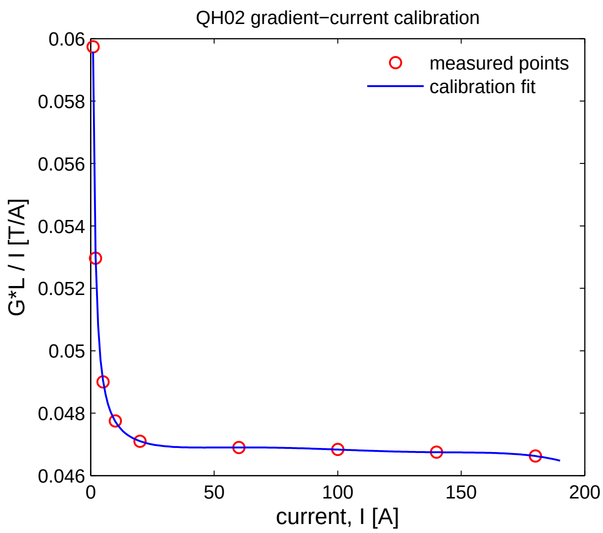


Figure 2: Integrated gradient over current factor for quadupole QH02.

## POWER SUPPLY WAVEFORMS

The waveforms used in the power supplies are pure sinusoidal based on the model calibrations. The injection is performed 14 ms after the minimum (injection "on the fly") and it was necessary to edit some points in two families of quadrupoles (QH02 and QV02) in the first milliseconds after the injection to maintain the tunes within $\pm 0.05$ and compensate the different nonlinear behaviour at low energy of the quadrupoles and the dipoles.

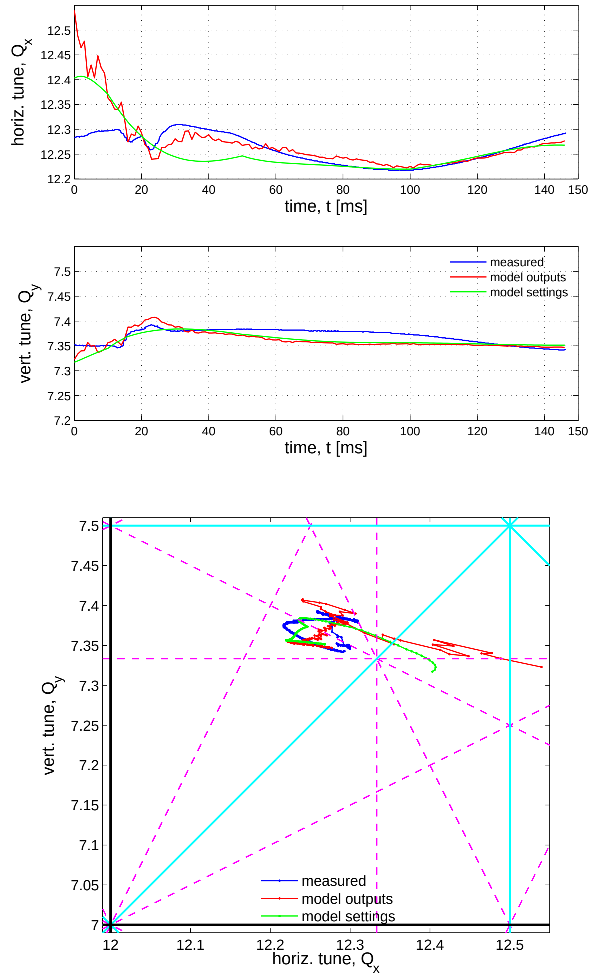


Figure 3: Movement of the working point during the ramp against the time (top) and plotted in the resonance diagram (bottom). The tunes measured from turn-by-turn data (blue line) are compared with the tune simulated with the model from the read-back currents (red line) and from the set currents (green line) of the digital power supplies.

## TUNE MEASUREMENTS

Figure 3 shows the comparison of the tunes given by the model and the measurements along the ramping. The tunes are calculated introducing in the model two current values: the set values of the waveforms, i.e. the pure sinusoidal edited in two points, and the measured output currents from the power supplies.

In the horizontal plane the tunes after the first 20 ms agree within 0.05, while the discrepancy at low energy is due to several factors as the remanent fields and the power supply offsets, tracking errors of the power supplies at low current and the precision of their measurement.

In the vertical plane the agreement is very good all along the ramp, because most of the vertical focusing is produced by the combined dipoles where the strength of the gradient scales as the dipole field that determines the beam energy.

## CHROMATICITY MEASUREMENTS

The total chromaticity of a synchrotron is the sum of three different terms: the natural chromaticity created by the quadrupoles, the term due to the sextupoles used to control the chromaticity, the term generated by the eddy currents induced in the metallic vacuum chamber of the dipoles during the ramp.

In the ALBA booster, the natural chromaticity is corrected by the built-in sextupole component of the combined bending magnets to (+1, +1). There are two additional sextupole families to control the chromaticity along the ramp, that at the moment are not used in the ramping.

Measurements of the chromaticity along the ramping were carried out by varying the RF $\pm 1$ kHz. The agreement between the measured and the theoretical chromaticity including the three terms is quite good, apart from the low energy values (Fig. 4). Below 1 GeV we realized that the tune shift due to the RF change was hard to be detected because of the strong chromaticity (see [5]). At energy higher than 1 GeV, the model agrees with the measurements within $\pm 0.5$.

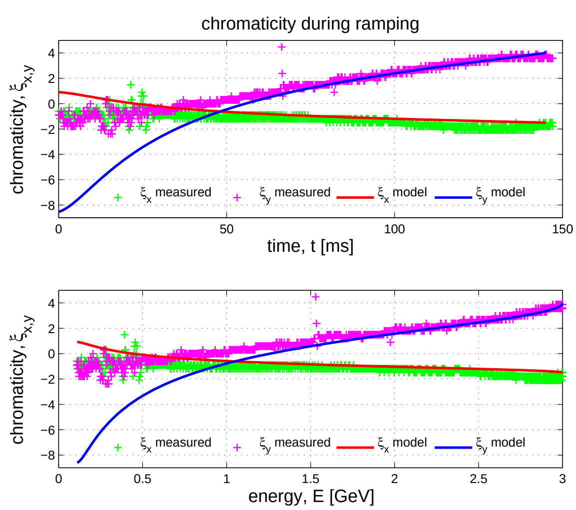


Figure 4: The measured and the theoretical horizontal and vertical chromaticity along the ramp as a function of the time (top) and of energy (bottom).

## EMITTANCE MEASUREMENTS

Emittance measurements along the ramp are performed at a synchrotron radiation monitor [6]. The CCD camera trigger is changed at every shot to measure the beam size at the desired time along the ramp.

Figure 5 shows that during the first part of the acceleration, the injected emittance decreases at two different rates corresponding to the adiabatic and radiation damping (first and second terms in Eq. 4). During the second part of the acceleration, the emittance increases due to the quantum excitation term (third term in Eq. 4) and stabilizes to the equilibrium value given by the booster optics.

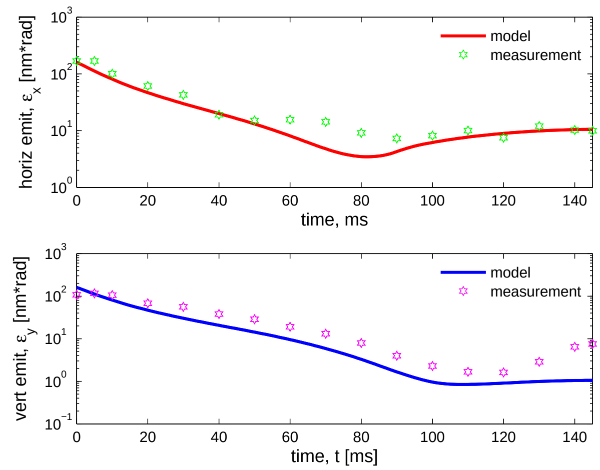


Figure 5: Horizontal (top) and vertical (bottom) emittance measurements during the ramp compared with the model.

$$\frac{d\epsilon_x}{dt} = -\epsilon_x \left( \frac{\dot{E}}{E} + \frac{2}{\tau_x} \right) + G_x \qquad (4)$$

The emittance calculation in the horizontal plane also includes the evolution of the energy spread.

In the vertical plane, the absence of quantum excitation produces a decrease during the whole ramp until it gets to a stable value given by the coupling, which is not presently evaluated. Note that the vertical measure shows an increase at the end of the ramp, which is not yet understood and is currently being investigated. The final emittances inferred from the beam size are (9.9, 7.5) nm·rad. While the horizontal value compares rather well with the model, the vertical plane shows a significant discrepancy at the end of the ramp.

## REFERENCES

[1] M. Pont et al., “Operation of the ALBA Injector”, these proceedings.

[2] G. Benedetti, D. Einfeld, Z. Martí, M. Muñoz, M. Pont, “Beam Optics Measurements during the commissioning of the ALBA booster”, IPAC’10, Kyoto, 2010.

[3] G. Benedetti, D. Einfeld, Z. Martí, M. Muñoz, M. Pont, “Optics for the ALBA booster synchrotron”, EPAC’08, Genoa, 2008.

[4] U. Iriso, F. Pérez, A. Salom, “Tune Measurement System at the ALBA Booster Commissioning”, BIW10, Santa Fe, 2010.

[5] Y. Papaphilippou et al., “Chromaticity Measurement in the ESRF Booster”, PAC’03, Portland, 2003.

[6] U. Iriso et al., “Diagnostics during the ALBA Booster Commissioning”, BIW10, Santa Fe, 2010.